

1 **Ozone Comparison between Pandora #34, Dobson #061, OMI, and OMPS at Boulder**  
2 **Colorado for the period December 2013 – December 2016.**

3  
4 **Jay. Herman<sup>1</sup>, Robert Evans<sup>4</sup>, Alexander Cede<sup>3</sup>, Nader Abuhassan<sup>1</sup>, Irina.**  
5 **Petropavlovskikh<sup>2</sup>, Glenn McConville<sup>2</sup>, Koji Miyagawa<sup>5</sup>, and Brandon Noiro<sup>2</sup>**

6  
7 <sup>1</sup> University of Maryland Baltimore County (JCET) at Goddard Space Flight Center, Greenbelt,  
8 MD

9 <sup>2</sup> NOAA Earth System Research Laboratory, Boulder, CO. Cooperative Institute for Research in  
10 Environmental Sciences (CIRES), University of Colorado, Boulder, CO

11 <sup>3</sup> LuftBlick, Austria and Goddard Space Flight Center, Greenbelt, MD

12 <sup>4</sup>Former scientist at NOAA/ESRL/GMD, Boulder, CO: Retired

13 <sup>5</sup>Guest Scientist at NOAA/ESRL/GMD, Boulder, CO

14  
15 **Abstract**

16 A one-time calibrated (in December 2013) Pandora Spectrometer Instrument (Pan #034) has  
17 been compared to a periodically calibrated Dobson spectroradiometer (Dobson #061) co-located  
18 in Boulder, Colorado, and compared with two satellite instruments over a 3-year period. The  
19 results show good agreement between Pan#034 and Dobson#061 within their statistical  
20 uncertainties. Both records are corrected for ozone retrieval sensitivity to stratospheric  
21 temperature variability obtained from the Global Modeling Initiative (GMI) and Modern-Era  
22 Retrospective analysis for Research and Applications (MERRA-2) model calculations.  
23 Pandora#034 and Dobson#061 differ by an average of  $2.1 \pm 3.2 \%$  when both instruments use  
24 their standard ozone absorption cross sections in the retrievals algorithms. The results show a  
25 relative drift ( $0.2 \pm 0.08\%$  per year) between Pandora observations against NOAA Dobson in  
26 Boulder, CO over a three-year period of continuous operation. Pandora drifts relative to the  
27 satellite Ozone Monitoring Instrument OMI and the Ozone Mapping Profiler OMPS are  $+0.18 \pm$   
28  $0.2 \%$  per year and  $-0.18 \pm 0.2 \%$  per year, respectively, where the uncertainties are 2 standard  
29 deviations. The drift between Dobson #061 and OMPS for a 5.5-year period (January 2012 –  
30 June 2017) is  $-0.07 \pm 0.06 \%$  per year.

31 Author(s): Jay Herman et al.

32 MS No.: amt-2017-157

33 MS Type: Research article

34 Iteration: Revised

35 Special Issue: Quadrennial Ozone Symposium 2016 Status and trends of atmospheric ozone  
36 (ACP/AMT inter-journal SI)

37  
38

39 **Introduction**

40 A Pandora Spectrometer Instrument #034 (PSI) located on top of the NOAA building in  
41 Boulder, Colorado has been operating since December 2013 with little maintenance and using  
42 the original calibration. The purpose of this paper is to present a comparison between two co-  
43 located ozone measuring instruments, Pandora #034 and Dobson #061 for the period December  
44 2013 to December 2016. Additional comparisons are made with satellite overpass data from  
45 OMI (Ozone Monitoring Instrument on board the AURA spacecraft) and OMPS (Ozone  
46 Mapping Profiler Suite on board the Suomi NPOESS satellite). This paper is an extension of a  
47 previously published paper (Herman et al., 2015) that presented just 1 year of data. The results  
48 demonstrate the accuracy and stability of both the Dobson and PSI for retrieval of total column  
49 ozone, and serves as a validation demonstration at one location for both the fairly new PSI and  
50 for satellite ozone data from OMI and OMPS. Part of the experiment comparing Pandora #034 to  
51 Dobson #061 was to see if Pandora #034 would perform well over a long period without  
52 additional calibration or adjustments. The only change made during the period 2014 to the  
53 present (August 2017) was to replace a broken motor on the suntracker that caused a data gap in  
54 early 2016.

55  
56 The characteristics of both the PSI and the Dobson Spectroradiometer are described in  
57 Herman et al. (2015). Briefly, the PSI consists of a small Avantes low stray light spectrometer  
58 (280 – 525 nm with 0.6 nm spectral resolution with 5 times oversampling) connected to an  
59 optical head by a 400 micron core diameter single strand fiber optic cable. The spectrometer is  
60 temperature stabilized at 20<sup>o</sup>C inside of a weather resistant container. The optical head consists  
61 of a collimator and lens giving rise to a 2.5<sup>o</sup> FOV (field of view) FWHM (Full Width Half  
62 Maximum) with light passing through two filter wheels containing diffusers, open hole, a UV340  
63 filter (blocks visible light), neutral density filters, and an opaque position (dark current  
64 measurement). The optical head is connected to a small suntracker capable of accurately  
65 following the sun’s center using a small computer-data logger contained in a weatherproof box  
66 along with the spectrometer. Pandora#034 is capable of obtaining NO<sub>2</sub> and Total Column Ozone  
67 TCO amounts sequentially over a period of 80 seconds. The integration time in bright sun is  
68 about 4 milli-seconds that is repeated and averaged for 30 seconds to obtain very high signal to  
69 noise and an ozone precision of less than 1 DU or 0.2% (1 DU = 2.69x10<sup>16</sup> molecules/cm<sup>2</sup>).

70  
71 The Dobson record in Boulder started in 1966 based on an improved design from the  
72 instrument first deployed in the 1920’s (Dobson, 1931). Dobson instrument is using differential  
73 absorption method to derive total column ozone from direct–sun measurements using two UV  
74 wavelength pairs in the 300 – 340 nm range (see Herman et al., 2015). The extensive Dobson  
75 network uses the Bass-Paur (BP) ozone absorption cross sections (Bass and Paur, 1985) for  
76 operational data processing (Komhyr et al., 1993).

77  
78

79 All NOAA Dobson instruments are periodically calibrated against WMO world standard  
80 Dobson #083, which in turn uses Langley method calibrations at the Mauna Loa Observatory  
81 station (Komhyr et al., 1989). Standard lamps are used to check Dobson spectral registration  
82 stability. Recently, July 2017, intermediate calibrations were applied to the Dobson #061 ozone  
83 data record that improved its comparison with satellite data (the calibration updates were  
84 processed by one of the co-authors, Koji Miyagawa).

85  
86 The main sources of noise in the PSI measurement comes from the presence of clouds or  
87 haze in the FOV, which increases the exposure time needed to fill the CCD wells to 80% and  
88 reduces the number of measurements in 20 seconds. For this comparison study, data were  
89 selected for scenes that are clear-sky conditions as determined from the Dobson A-D pair direct-  
90 sun data record.

91  
92 Accuracy in the PSI spectral fitting retrieval is obtained using careful measurements of the  
93 spectrometer's slit function, wavelength calibration, and knowledge of the solar spectrum at the  
94 top of the atmosphere. The current operational PSI ozone retrieval algorithm used in this study is  
95 based on extraterrestrial solar flux from a combination of the Kurucz spectrum (wavelength  
96 resolution  $\lambda/1\lambda = 500\ 000$ ) radiometrically normalized to the lower-resolution shuttle Atlas-3  
97 SUSIM spectrum (Van Hoosier, 1996; Bernhard et al., 2004, 2005), BDM ozone cross sections  
98 (Brion et al. (1993, 1998) and Malicet et al. (1995)), corrections for stray light, and an effective  
99 ozone weighted temperature.

100  
101 The Dobson data used in this study contain the individual measurements (more than 1 per  
102 day between 09:00 and 15:00 local time with almost all of the data between 10:00 and 14:00) for  
103 clear-sky direct-sun observations using the quartz plate and A-D wavelength pairs for ozone  
104 retrieval. These were made available by one of the co-authors (I. Petropavlovskikh, private  
105 communication, Table 2). The NOAA Dobson total ozone data are typically archived at  
106 WOUDC (World Ozone and Ultraviolet Radiation Data Centre) or NDACC (Network for the  
107 Detection of Atmospheric Composition Change) with one representative ozone value per day.

## 108 109 **1. Temperature Sensitivity**

110  
111 The PSI ozone retrieval algorithm is more sensitive to the effective ozone weighted  
112 average temperature than is the 4 wavelength Dobson retrieval (Redondas et al., 2014).  
113 Neglecting the temperature sensitivity creates a seasonal difference between the two instruments.  
114 To correct for this, we use an effective ozone temperature  $T_E$  based on daily ozone weighted  
115 altitude temperature averages (Redondas et al., 2014). The temperature and ozone profile data  
116 were obtained from the GMI (Global Modeling Initiative) model calculation for 2012 to 2016.  
117 (<https://gmi.gsfc.nasa.gov/merra2hindcast/>). The GMI model provides atmospheric composition  
118 hindcasts using MERRA-2 (Modern-Era Retrospective analysis for Research and Applications,

119 Version 2, meteorology (Strahan et al., 2013; Wargan and Coy, 2012)  
 120 <https://gmao.gsfc.nasa.gov/reanalysis/MERRA-2/>). The simulation with 2 x 2.5 degree resolution  
 121 uses the CCMI (Chemistry–Climate Modelling Initiative, Morgenstern et al., 2017) emissions  
 122 and boundary conditions. MERRA-2 uses assimilation schemes based on hyperspectral radiation,  
 123 microwave observations and ozone satellite measurements. The resulting seasonal cycle for  $T_E$   
 124 shows variations over the four year period, while day-to-day variability is enhanced during  
 125 winter and spring season (Fig. 1). An estimated 5<sup>th</sup> year (2017) has been added (Fig. 1) by  
 126 forming the average of the daily temperatures from the 2013 to 2016 period.

127  
 128 The  $T_E$  time series data are used for an ozone retrieval temperature correction  $TCO_{corr}$   
 129 coefficient per  $^{\circ}K$  given in the form  $TCO_{corr} = TCO (1 + C(T))$  and  $O_3(corr) = O_3 TCO_{corr}$   
 130 (Herman et al., 2015), where  $C(T_E)$  is given by eqns. 1 and 2.

131

$$C_{\text{Pandora-BDM}}(T_E) = 0.00333(T_E - 225) \quad (\text{Herman et al., 2015}) \quad (1)$$

$$C_{\text{Dobson-BP}}(T_E) = -0.0013(T_E - 226.7) \quad (\text{Redondas et al., 2014}) \quad (2)$$

$$C_{\text{Dobson-BDM}}(T_E) = 0.00042(T_E - 226.7) \quad (\text{Redondas et al., 2014}) \quad (3)$$

132 As mentioned earlier, the Dobson TCO retrieval normally uses the Bass and Paur (BP)  
 133 ozone absorption coefficients, while Pandora uses the Brion-Daumont-Maliget (BDM)  
 134 coefficients. A change in  $T_E$  of  $+1^{\circ}$  change leads to TCO changes for the Pandora(BDM),  
 135 Dobson(BP), and Dobson(BDM) instruments of  $+0.33\%$ ,  $-0.13\%$ , and  $0.042\%$ , respectively.  
 136 For a nominal TCO value of 325 DU, the change would be  $+1.1$  and  $-0.4$  DU, a net relative  
 137 change of 1.5 DU for a  $1^{\circ}K$  change between Pandora(BDM) and Dobson(BP).

138

139 While BDM cross sections are not currently recommended for use in standard Dobson  
 140 processing, their use yields slightly different values of TCO and a smaller sensitivity to  
 141 temperature. The basic Dobson algorithm, based on pairs of wavelengths, is intrinsically less  
 142 sensitive to  $T_E$  than Pandora's spectral fitting retrieval.

143

## 144 **2. TCO Comparisons between Pandora, Dobson, OMI and OMPS**

145

146 Comparing retrieved TCO from the PSI, Dobson, OMI and OMPS instruments show that  
 147 there are small, but significant differences between the PSI and Dobson instruments and between  
 148 the ground-based instruments and satellite derived values of TCO. The difference is calculated  
 149 using three-year estimates of secular change based on a linear least squares fit to the percent  
 150 differences between the instruments. The cloud-free direct-sun A-D pair Dobson ozone data are  
 151 selected for comparison with time-matched Pandora#034 retrieved ozone data (Herman et al.,  
 152 2015). The Pandora#034 retrieved ozone (every 80 seconds) are matched to the less frequent  
 153 Dobson#061 retrieval times that are obtained for mid-day solar zenith angles (SZAs) and

154 averaged over  $\pm 8$  minutes (Fig. 2A).

155  
156 Each clear-sky PSI data point is an average of 2000 (early morning to evening SZAs) to  
157 4000 (mid-day SZAs) measurements obtained during 20 seconds. All data for this study were  
158 clear-sky within the instrument's field of view based on the Dobson criteria for A-D-pair direct-  
159 sun clear sky. In addition, the PSI data are averaged over a period of  $\pm 8$  minutes surrounding  
160 the Dobson time of measurement (2 to 3 times per day). Since PSI measurements are obtained  
161 every 80 seconds, there were an additional 10 PSI data points averaged together to compare to  
162 each Dobson, OMI, or OMPS measurement. The result is high signal to noise values for Pandora  
163 and high precision (0.1%). The same procedure using cloud-screened PSI data was used for  
164 comparisons with OMI and OMPS, where they measure once or twice per day over Boulder,  
165 Colorado. Some of the variations in the day to day ozone values are driven by changes in the  
166 local weather over Boulder, Colorado (see Fig. 14 in Herman et al., 2015), with weekly averages  
167 having much smaller variation.

168  
169 Figure 2B shows a Lowess(0.1) fits to the two time series in Fig. 2A that is approximately  
170 equivalent to a 3-month running average. The Lowess(f) procedure is based on local least  
171 squares fitting using low order polynomials applied to a specified fraction f of the data  
172 (Cleveland, 1979) that reduces the effect of outlier points from the mean. The smooth curves  
173 show a small variable difference between the Dobson and Pandora time series. Fig. 2C shows the  
174 percent difference PD between the time series in Fig. 2A and the residual seasonal variation in  
175 PD. Estimating the slope of the least squares fit to the percent difference is sensitive to the  
176 selection of the end points of the time series. This effect can be minimized by removing the  
177 seasonal time dependence (Fig. 2C) using a low-pass filter function with zero slope derived from  
178 the Lowess(0.1) fit. The result is shown in Fig. 3A.

179  
180 Figure 3 shows the de-seasonalized percent differences PD(A,B) for six pairs between  
181 Pandora #034, Dobson #061, OMI, and OMPS for the 3-year period 2014 – 2016 (summarized in  
182 Table 1). The slightly curvy Lowess (0.1) lines about each linear fit show the residual seasonal  
183 cycles, which are too small to have an effect on slope determination. Error estimates (Fig. 3 and  
184 Table 1) for the linear least squares slopes and averages are one standard deviation (1-STD).  
185 Some of the error estimates are large enough to make the statistical significance of the slopes  
186 marginal (see Panel E OMPS vs Pandora;  $0.18 \pm 0.098$ ,  $p = 0.06$ ), while others are significant  
187 (see Panel D OMI vs Dobson:  $-0.18 \pm 0.08$ ,  $p = 0.03$ ) at the 2-STD level. The significance  
188 probability parameter p is given, where p is the probability (0 to 1) that the slope is statistically  
189 different from 0 relative to  $p = 0.05$ . Also shown are the numbers of data points in each time  
190 series.

191  
192 After removal of the residual seasonal variation in the calculated percent differences,  
193 there still is a statistically significant drift of 0.2% per year ( $p < 0.001$ ) between the Pandora#034

194 and Dobson#061 (Panels A and B in Fig. 3) using either BP or BDM ozone cross sections for the  
195 Dobson. The differences in the mean values (-2.1 and -2.8%) are not significant at the 2-STD  
196 level.

197  
198 The linear trend (Panel C,  $-0.09 \pm 0.08$  % per year,  $p = 0.3$ ) between the Dobson and  
199 OMPS is not significantly different from zero, while the drift with OMI (Panel D,  $-0.18 \pm 0.08$  %  
200 per year,  $p = 0.03$ ) is significant. This suggests that OMI ozone retrievals are drifting with  
201 respect to OMPS and the Dobson. Extending the period from 2012 to June 2017 gives a very  
202 small, but significant trend,  $-0.07 \pm 0.03$  % per year,  $p = 0.047$  for PD(OMPS,Dobson).

203  
204 Calculations for Pandora#034 (Panels E and F in Fig. 3) show marginally significant ( $p =$   
205  $0.06$ ) trends for Pandora#034 compared to OMPS (Panel E,  $-0.18 \pm 0.098$  % per year) and OMI  
206 (Panel F,  $+0.18 \pm 0.096$  % per year). If the Pandora#034 time series is extended into 2017 to  
207 minimize the effect of missing Pandora data in 2016, then the trends for Pandora compared to  
208 OMPS ( $-0.2 \pm 0.08$  % / Year  $p = 0.013$ ) and OMI ( $0.15 \pm 0.076$   $p=0.05$ ) are significant, but not  
209 different from the shorter 2014 – 2016 period. The secular trends for the difference between  
210 Pandora#034 and Dobson#061 ( $-0.2\%$  per year) are almost the same for both Dobson BP and  
211 BDM ozone absorption coefficients even though the temperature sensitivity using the Dobson  
212 BDM ozone absorption coefficients is small ( $0.042\%$  per  $^{\circ}\text{C}$ ). This suggests that the  
213 stratospheric effective ozone temperature change is not a source for the small difference between  
214 Pandora#034 and Dobson#061.

215  
216 Figure 4 shows that the TCO between Pandora#034 and Dobson#061 are highly  
217 correlated with 1:1 slope and the correlation coefficient  $r^2 = 0.97$  for the 3-year period 2014 to  
218 2016. Similar correlation plots (Fig. 5) for Pandora#034 and Dobson#061 with OMI and OMPS  
219 also show very high correlations. The correlations in TCO are obtained after only temperature  
220 corrections to Pandora#034 and Dobson#061 using  $T_E$  (TCO pairs similar to Fig. 2, panel A).

221  
222 The Pandora, OMI, and OMPS data used in this study are from the overpass files located  
223 on the public websites (Table 2).

## 224 225 **Summary**

226 Temperature corrected Pandora#034 and Dobson#061 differ by an average of 2.1% with  
227 Pandora using its standard retrieval BDM ozone absorption cross sections and Dobson using the  
228 recommended BP ozone absorption cross sections. Pandora compared to Dobson shows a small,  
229 but significant drift ( $-0.2 \pm 0.04$  % per year,  $p < 0.001$ ) for the 2014 – 2016 period. Comparisons  
230 of Pandora with OMI and OMPS are marginally significant drifts of  $0.18 \pm 0.1$  and  $-0.18 \pm 0.1$   
231  $p=0.06$  for 2014-2016, but are significant ( $0.15 \pm 0.076$  % per year,  $p=0.05$  and  $-0.2 \pm 0.08$  % per  
232 year,  $p = 0.013$ , respectively) if the period is extended to mid-2017 to minimize the effect of  
233 missing Pandora data during 2016. The small Pandora and Dobson trends compared to OMPS  
234 suggests that both instruments are stable. The conclusion is that the periodically calibrated

235 Dobson#061 is able to detect smaller ozone trends than a Pandora instrument with no  
236 intermediate calibration during a 3-year period. The longer term trend for Dobson compared to  
237 OMPS for a 5.5-year period (2012 – June 2017) is  $-0.07 \pm 0.03$  % per year,  $p = 0.047$ .

238  
239 **Acknowledgement:** The authors would like to thank Dr. Susan Strahan and the MERRA-2 team  
240 for supplying the atmospheric temperature data for Boulder, Colorado.

241  
242  
243

#### 244 **References**

245 Bass, A. M. and Paur, R. J.: The ultraviolet cross-sections of ozone, I, The measurements, in:  
246 Atmospheric Ozone, edited by: Zerefos, C. S., Ghazi, A., and Reidel, D., Norwell, Mass., 606–  
247 610, 1985.

248  
249 Bernhard, G., Booth, C. R., and Ehramjian, J. C.: Version 2 data of the National Science  
250 Foundation’s Ultraviolet Radiation Monitoring Network: South Pole, *J. Geophys. Res.*, 109,  
251 D21207, doi:10.1029/2004JD004937, 2004.

252  
253 Bernhard, G., Evans, R. D., Labow, G. J., and Oltmans, S. J.: Bias in Dobson total ozone  
254 measurements at high latitudes due to approximations in calculations of ozone absorption  
255 coefficients and air mass, *J. Geophys. Res.*, 110, D10305, doi:10.1029/2004JD005559, 2005.

256 Brion, J., Chakir, A., Daumont, D., Malicet, J., and Parisse, C.: High-resolution laboratory  
257 absorption cross section of O<sub>3</sub> Temperature effect, *Chem. Phys. Lett.*, 213, 610–612, 1993.

258  
259 Brion, J., Chakir, A., Charbonnier, J., Daumont, D., Parisse, C., and Malicet, J.: Absorption  
260 spectra measurements for the ozone molecule in the 350–830 nm region, *J. Atmos. Chem.*, 30,  
261 291–299, 1998.

262  
263 Cleveland, William S., Robust Locally Weighted Regression and Smoothing Scatterplots,  
264 *Journal of the American Statistical Association*, Vol. 74, No. 368. , pp. 829-836, 1979.

265  
266 Dobson, G. M. B. (1931), A photoelectric spectrophotometer for measuring the amount of  
267 atmospheric ozone, *Proc. Phys. Soc.*, 43, 324–339, 1931.

268  
269 Herman, J.R., R.D. Evans, A. Cede, N.K. Abuhassan, I. Petropavlovskikh, and G. McConville,  
270 Comparison of Ozone Retrievals from the Pandora Spectrometer System and Dobson  
271 Spectrophotometer in Boulder Colorado, *Atmos. Meas. Tech.*, 8, 3407–3418, 2015,  
272 doi:10.5194/amt-8-3407-2015.

273  
274 Komhyr, W. D., R. D. Grass, and R. K. Leonard (1989), Dobson spectrophotometer 83: A  
275 standard for total ozone measurements, 1962–1987, *J. Geophys. Res.*, 94(D7), 9847–9861,  
276 doi:10.1029/JD094iD07p09847, 1989.

277

278 Komhyr, W. D., C. L. Mateer, and R. D. Hudson (1993), Effective Bass-Paur 1985 ozone  
279 absorption coefficients for use with Dobson ozone spectrophotometers, *J. Geophys. Res.*,  
280 98(D11), 20451–20465, doi:10.1029/93JD00602, 1993.  
281

282 Malicet, J., Daumont, D., Charbonnier, J., Parisse, C., Chakir, A., and Brion, J.: Ozone UV  
283 spectroscopy. II. Absorption cross sections and temperature dependence, *J. Atmos. Chem.*, 21,  
284 263–273, 1995.  
285

286 Morgenstern, Olaf, Michaela I. Hegglin, Eugene Rozanov, Fiona M. O'Connor, N. Luke  
287 Abraham, Hideharu Akiyoshi, Alexander T. Archibald, Slimane Bekki, Neal Butchart, Martyn P.  
288 Chipperfield, Makoto Deushi, Sandip S. Dhomse, Rolando R. Garcia, Steven C. Hardiman, Larry  
289 W. Horowitz, Patrick Jöckel, Beatrice Josse, Douglas Kinnison, Meiyun Lin, Eva Mancini,  
290 Michael E. Manyin, Marion Marchand, Virginie Marécal, Martine Michou, Luke D. Oman,  
291 Giovanni Pitari, David A. Plummer, Laura E. Revell, David Saint-Martin, Robyn Schofield,  
292 Andrea Stenke, Kane Stone, Kengo Sudo, Taichu Y. Tanaka, Simone Tilmes, Yousuke  
293 Yamashita, Kohei Yoshida, and Guang Zeng, Review of the global models used within phase 1  
294 of the Chemistry–Climate Model Initiative (CCMI), *Geosci. Model Dev.*, 10, 639-  
295 671, <https://doi.org/10.5194/gmd-10-639-2017>, 2017.  
296

297 Redondas, A., Evans, R., Stuebi, R., Köhler, U., and Weber, M.: Evaluation of the use of five  
298 laboratory-determined ozone absorption cross sections in Brewer and Dobson retrieval  
299 algorithms, *Atmos. Chem. Phys.*, 14, 1635–1648, doi:10.5194/acp-14-1635-2014, 2014  
300

301 Strahan, S.E., A.R. Douglass, and P.A. Newman (2013), The contributions of chemistry and  
302 transport to low Arctic ozone in March 2011 derived from Aura MLS Observations, *J. Geophys.*  
303 *Res.*, 118, doi:10.1002/jgrd.50181, 2013.  
304

305 Van Hoosier, M. E.: Solar ultraviolet spectral irradiance data with increased wavelength and  
306 irradiance accuracy, *SPIE Proceedings*, 2831, 57–64, 1996.

307 Wargan, K. and L. Coy, 2016: Strengthening of the Tropopause Inversion Layer during the 2009  
308 Sudden Stratospheric Warming: A MERRA-2 Study. *Journal of the Atmospheric Sciences*, 73,  
309 1871–1887, doi: 10.1175/JAS-D-15-0333.1, 2016.  
310  
311  
312  
313



314 **Tables**

315

Table 1 Percent Difference Summary of Linear Fit Slopes and Mean Differences in Fig. 3

Percent Diff(A,B)	Slope (% per Year)	Probability	Mean (%)	Points	Panel
Pan, Dob(BP)	-0.2 ± 0.04	P < 0.001	-2.1 ± 1.6	2020	A
Pan, Dob(BDM)	-0.2 ± 0.04	P < 0.001	-2.8 ± 1.6	2020	B
OMPS, Dob(BP)	-0.09 ± 0.08	P = 0.3	-1.4 ± 2.1	854	C
OMI, Dob(BP)	-0.18 ± 0.08	P = 0.03	-1.4 ± 1.9	654	D
OMPS, Pan	-0.18 ± 0.098	P = 0.06	0.96 ± 2.7	952	E
OMI, Pan	+0.18 ± 0.096	P = 0.06	1.1 ± 2.1	624	F

316

317

318

319

Table 2 Data Availability

**OMI:**

[https://avdc.gsfc.nasa.gov/index.php?site=1593048672&id=28/aura\\_omi\\_l2ovp\\_omto3\\_v8.5\\_boulder.co\\_067.txt](https://avdc.gsfc.nasa.gov/index.php?site=1593048672&id=28/aura_omi_l2ovp_omto3_v8.5_boulder.co_067.txt)

**OMPS:**

[ftp://toms.gsfc.nasa.gov/pub/omps\\_tc/overpass/suomi\\_npp\\_omps\\_l2ovp\\_nmto3\\_v02\\_boulder.co\\_067.txt](ftp://toms.gsfc.nasa.gov/pub/omps_tc/overpass/suomi_npp_omps_l2ovp_nmto3_v02_boulder.co_067.txt)

**Pandora34:**

<https://avdc.gsfc.nasa.gov/pub/DSCOVER/Pandora/DATA/Boulder/Pandora34/L3c/>

**Dobson061:**

[ftp://aftp.cmdl.noaa.gov/data/ozwv/Dobson/WinDobson/Pandora%20comparisons/Dobson61%20Boulder%20Ad-dsgqp%20120213-032717\\_w\\_Header.txt](ftp://aftp.cmdl.noaa.gov/data/ozwv/Dobson/WinDobson/Pandora%20comparisons/Dobson61%20Boulder%20Ad-dsgqp%20120213-032717_w_Header.txt)

320 **Figure Captions**

321 Fig. 1 Calculated  $T_E$  using model estimates of  $O_3$  and temperature profiles. The Trend is  
322 calculated from the difference of  $T_E$  from its 4-year daily mean that is also used for year 2017  
323 labelled Avg.

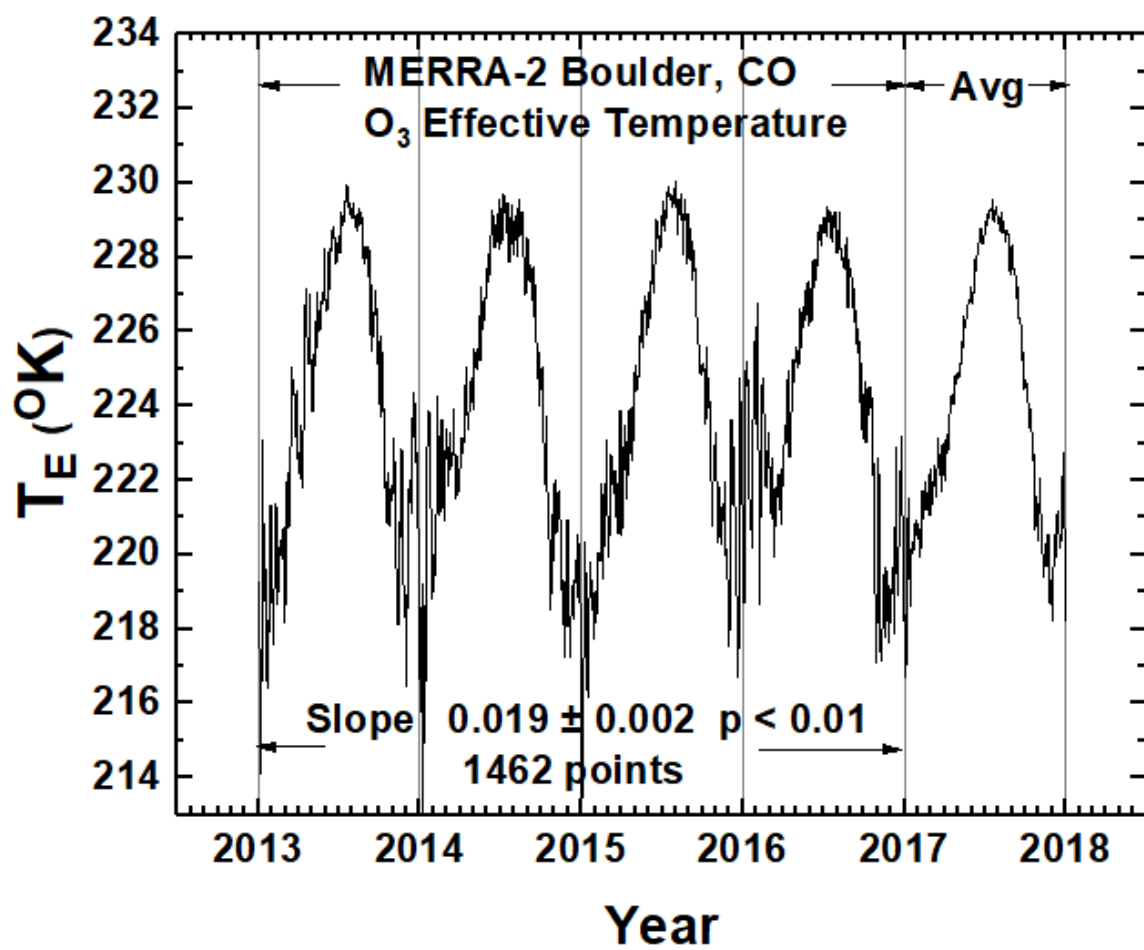
324  
325 Fig. 2 Panel A shows the retrieved ozone time series (December 2013 – June 2017) for Pandora  
326 (red) and Dobson (Black). Panel B shows Lowess(0.1) fit to the each time series. Panel C shows  
327 the percent difference, a linear least squares fit, and a Lowess(0.1) fit showing seasonal residuals.  
328

329 Fig. 3 Comparisons of Pandora(BDM) with Dobson(BP) retrieved ozone for Boulder, Colorado  
330 in percent differences of retrieved ozone and comparisons with OMI and OMPS. Slope = value  
331 of the linear least square fit,  $\pm N$  is 1 STD, and  $p$  is the probability (0 to 1) that the slope is  
332 statistically different from 0 relative to  $p = 0.05$ . The solid lines are a Lowess(0.1) fit and a linear  
333 least squares fit.

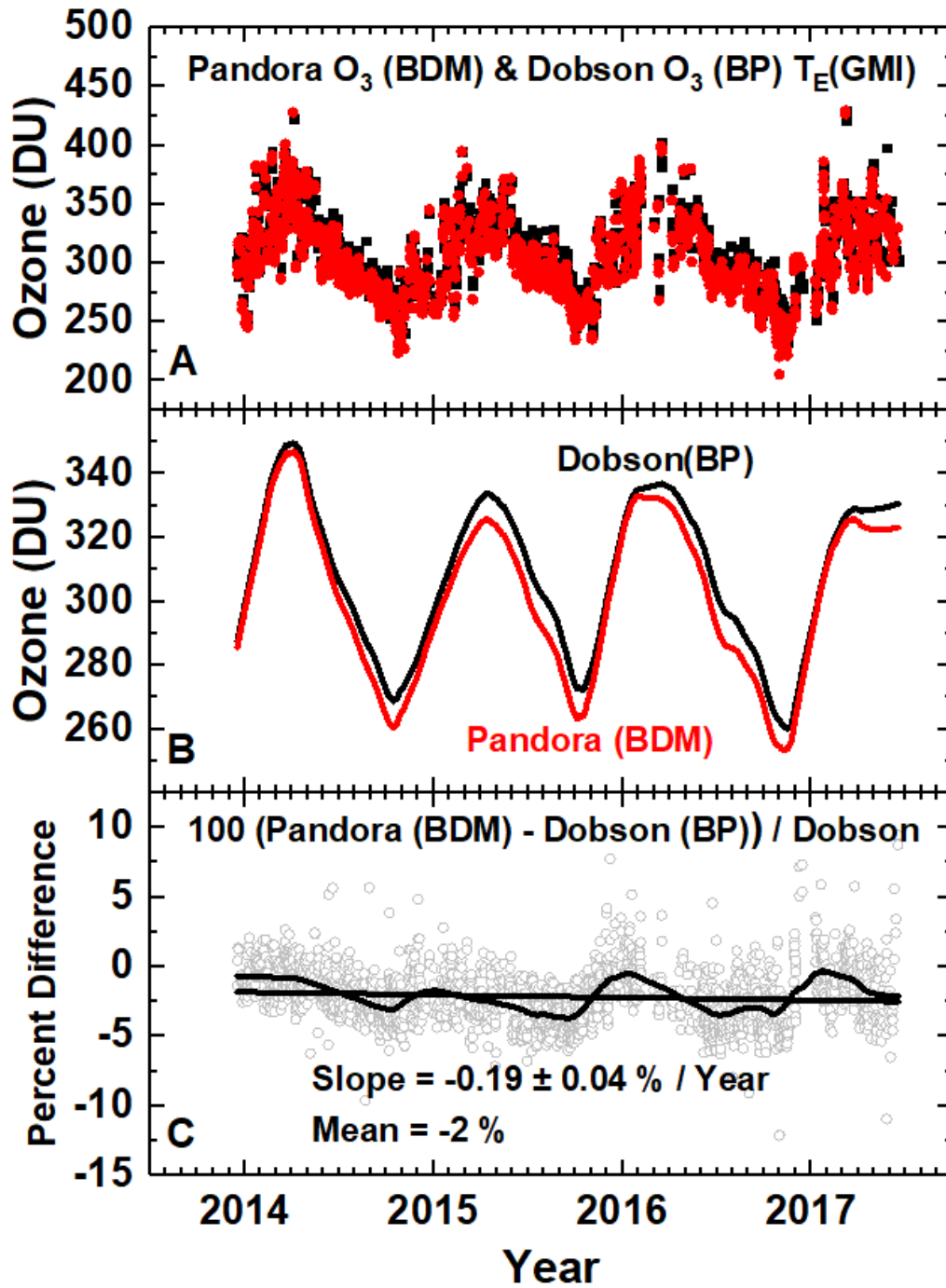
334  
335 Fig. 4 Correlation between Pandora #034 and Dobson #061: 2014 – 2016

336  
337 Fig. 5 Correlation of Pandora#034 and Dobson#061 with OMI and OMPS: 2014 - 2016

338 **Figures**  
339

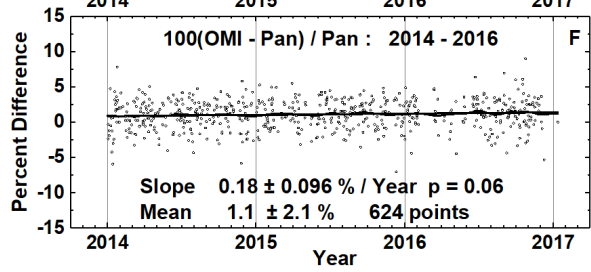
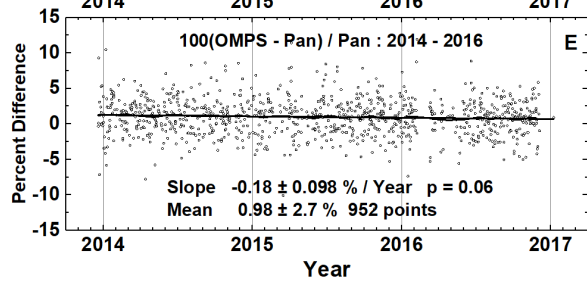
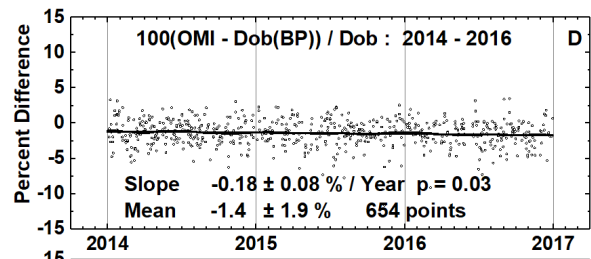
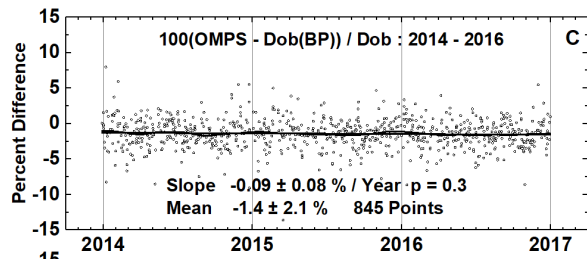
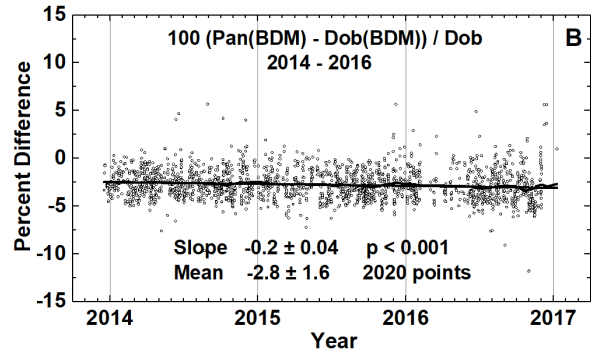
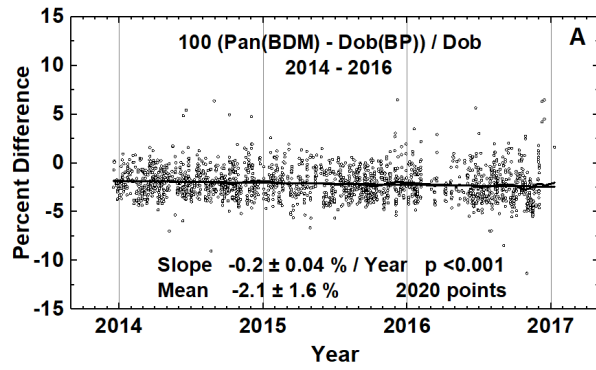


340  
341 **F1**



342 **F2**

343



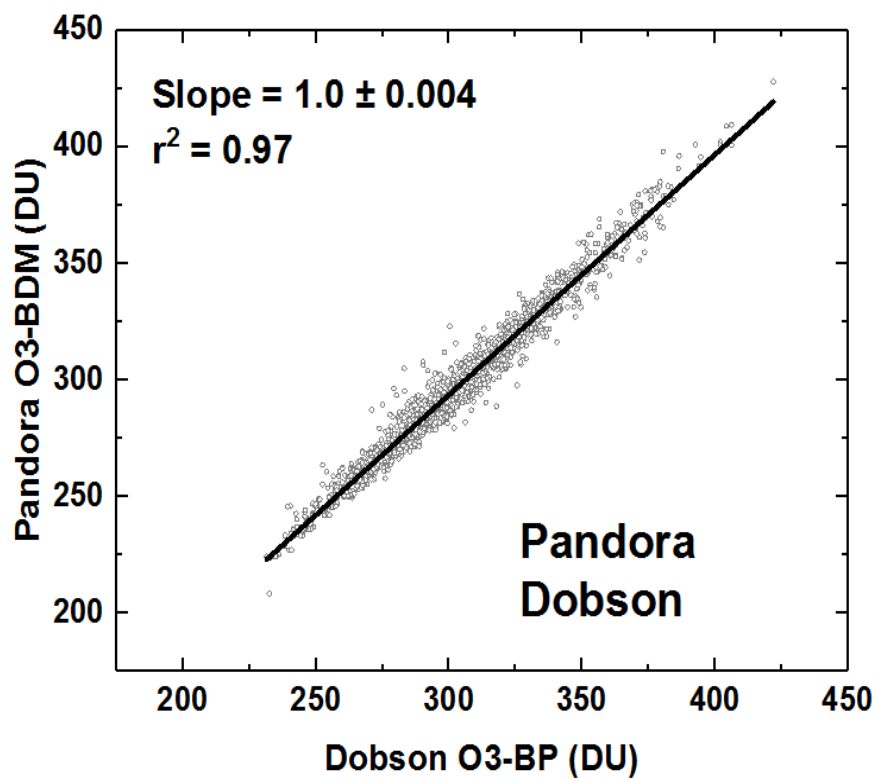
344

345

346 **F3**

347

348



349

350

351 **F4**

